Parametric spatiotemporal oscillation in reaction-diffusion systems

Shyamolina Ghosh and Deb Shankar Ray*
Indian Association for the Cultivation of Science, Jadavpur, Kolkata-700032, India
(Received 30 December 2015; revised manuscript received 10 February 2016; published 7 March 2016)

We consider a reaction-diffusion system in a homogeneous stable steady state. On perturbation by a time-dependent sinusoidal forcing of a suitable scaling parameter the system exhibits parametric spatiotemporal instability beyond a critical threshold frequency. We have formulated a general scheme to calculate the threshold condition for oscillation and the range of unstable spatial modes lying within a V-shaped region reminiscent of Arnold's tongue. Full numerical simulations show that depending on the specificity of nonlinearity of the models, the instability may result in time-periodic stationary patterns in the form of standing clusters or spatially localized breathing patterns with characteristic wavelengths. Our theoretical analysis of the parametric oscillation in reaction-diffusion system is corroborated by full numerical simulation of two well-known chemical dynamical models: chlorite-iodine-malonic acid and Briggs-Rauscher reactions.

DOI: 10.1103/PhysRevE.93.032209

I. INTRODUCTION

Periodic forcing of dynamical systems has been studied over many decades because of their implications in several areas of natural sciences [1,2]. An oscillatory system entrains to periodic perturbation for appropriate range of values of amplitude and frequency. The forcing with frequency ω_p may cause a shift of the system's characteristic frequency to a new value ω, so that entrainment may occur for rational ratios of numbers n, m such that $\omega_p/\omega = m/n$. The system may also exhibit quasiperiodic motion with irrational ratios for weak perturbation. Over the years the dynamical systems in zero dimension as well as with spatial extension have been investigated in the context of circadian cycles driven by sunlight [3–5], chemical patterns in photosensitive Belousov-Zhabotinsky (BZ) reaction [6,7], such as standing wave labyrinths [8] and rotating spirals [9,10] forced by light, small sinusoidal potential wave induced electrochemical material growth [11] exhibiting oscillatory Turing pattern, etc.

A closer look into the above-mentioned studies suggests that it is possible to categorize the forcing into two major types. First, the dynamical system is forced directly [12] as in the case of a forced oscillator; second, a suitable parameter of the oscillator, e.g., its characteristic frequency, is modulated by a time-periodic perturbation [13]. In the latter case the system undergoes parametric oscillation and is amenable to studies in terms of the Mathieu-Hill equation $\ddot{x} + a(t)x = 0$, where $a(t) = a(t + T)$ with $T = 2\pi/\omega_p$, the time period of the parameter $a(t)$. Depending on the amplitude, frequency locking may occur in such systems when the time period (T) or nT of the parameter matches with the frequency of the unforced system. Thus, a system in a Hopf state may exhibit complex mixed-mode oscillations under parametric perturbation [14]. Mixed-mode oscillatory patterns have been observed in periodically forced BZ reaction model in a parameter regime where the unforced system is excitable (i.e., with no sustained intrinsic oscillations) so that it has no intrinsic natural frequency [15]. An extended Oregonator model has been used to show how spatiotemporal chaos and intermittency may emerge out of mixed mode oscillations and breathing dynamics [16]. Reaction-diffusion systems also offer interesting candidates showing spatial localization but temporally breathing in this state [17].

A key aspect of the perturbed system is the consideration of the dynamical state under unforced condition. In the overwhelming majority of the studies on reaction-diffusion systems the state remains in an oscillatory state with a characteristic frequency [18]. The dynamics under such a condition is well described by the Ginzburg-Landau (GL) equation [19,20] near Hopf bifurcation. Such approach has been adopted, for example, in the treatment of response of Turing stripe patterns to a simple spatiotemporal forcing in the form of a traveling wave and is spatially resonant with characteristic Turing wavelength, leading to interesting symmetry breaking of striped patterns [21]. The object of the present paper is to explore the time-periodic parametric perturbation on a spatially extended dynamical system in a homogeneous stable steady state, a scenario that remains outside the scope of GL description. It has been shown when the forcing frequency matches twice the oscillation frequency of the forced system for the amplitude of forcing beyond a critical threshold, the system undergoes spatially stationary, temporal parametric oscillation. We have formulated a general scheme to derive the threshold frequency, which critically determines the range of wavelength for this parametric spatiotemporal instability. Our full numerical simulation results show that depending on the specificity of nonlinearity of the models, this instability may lead to patterns of various types. A typical one observed in the present study is a kind of standing clusters with fixed irregular spatial domains that oscillate periodically in time as demonstrated earlier in experiments with Belousov-Zhabotinsky reaction with global feedback [22]. We have also shown the occurrence of localized breathing patterns with characteristic wavelength. Our theoretical analysis is illustrated with the help of two specific well-known examples, chlorine-dioxide-iodine-malonic acid (CIMA) reaction [23–26] and iodine clock or Briggs-Rauscher reaction [27,28].

The outline of the paper is as follows. In Sec. II we have formulated a general scheme of parametric spatiotemporal oscillation of a reaction-diffusion system kept in a stable steady state. The major focus lies on deriving the threshold

*pcdsr@iacs.res.in

condition for oscillation. Section III is devoted to a perturbative analysis to identify the instability region which is a V-shaped Arnold's-tongue-like structure [29] for specific values of threshold frequency. In Sec. IV we have considered two specific examples. The paper is concluded in Sec. V.

II. SPATIOTEMPORAL PARAMETRIC OSCILLATION IN REACTION-DIFFUSION SYSTEMS: GENERAL SCHEME

To start with we consider an arbitrary reaction-diffusion system in two variables. The dynamical equations in two dimensions (x,y) can be written down as follows;

$$\dot{u} = f(u,v) + D_u\nabla^2 u, \quad \dot{v} = \tilde{b}G(u,v) + D_v\nabla^2 v, \tag{2.1}$$

where, $u(x,y,t)$ and $v(x,y,t)$ are the concentration of the two reacting species of a chemical reaction; D_u and D_v are the respective diffusion coefficients. $f(u,v)$ and $G(u,v)$ are, in general, nonlinear functions. $\tilde{b}$ is a constant parameter. The parametric variation is considered by making $\tilde{b}$ explicitly time dependent as follows:

$$\tilde{b}(t) = b + h\sin(\omega_p t), \tag{2.2}$$

where, b is the constant part and h and ω_p are the amplitude and frequency of the input time-dependent sinusoidal perturbation, respectively. Let (u_0,v_0) be the homogeneous steady state of the dynamical system. Linearization of the system around the steady state leads us to the time evolution of the small perturbation $(\delta u,\delta v)$ as given by;

$$\dot{\delta u} = f_u\delta u + f_v\delta v + D_u\nabla^2\delta u \tag{2.3}$$

$$\dot{\delta v} = \tilde{b}[G_u\delta u + G_v\delta v] + D_v\nabla^2\delta v. \tag{2.4}$$

Here, f_u, f_v and G_u, G_v are, as usual, the partial derivatives of functions $f(u,v)$ and $G(u,v)$ with respect to the variables u and v evaluated at the steady state (u_0,v_0). The steady state will be stable to spatially uniform perturbation if and only if, $(f_u + g_v) < 0$ and $(f_u g_v - f_v g_u) > 0$, with $g_u = bG_u$ and $g_v = bG_v$. From Eqs. (2.2) and (2.4) it follows;

$$\dot{\delta v} = [g_u + b_1\sin(\omega_p t)]\delta u + [g_v + b_2\sin(\omega_p t)]\delta v + D_v\nabla^2\delta v, \tag{2.5}$$

where,

$$b_1 = hG_u, b_2 = hG_v. \tag{2.6}$$

Assuming spatiotemporal perturbations δu and δv in two dimensions of the following forms

$$\delta u = \delta U(t)\cos(K_x x + K_y y),$$
$$\delta v = \delta V(t)\cos(K_x x + K_y y). \tag{2.7}$$

Equations (2.3) and (2.5) can be represented as

$$\dot{\delta U} = (f_u - D_u K^2)\delta U + f_v\delta V \tag{2.8}$$

$$\dot{\delta V} = [g_u + b_1\sin(\omega_p t)]\delta U + [(g_v - D_v K^2) + b_2\sin(\omega_p t)]\delta V \tag{2.9}$$

with $K_x^2 + K_y^2 = K^2$.

By differentiating Eq. (2.8) with respect to t and following elimination of δV terms from the resulting equation we write

$$\begin{aligned}\ddot{\delta U} &= (f_u - D_u K^2)\dot{\delta U} + f_v\dot{\delta V}\\ &= [f_u + g_v - (D_u + D_v)K^2 + b_2\sin(\omega_p t)]\dot{\delta U}\\ &\quad - [f_u g_v - f_v g_u - (f_u D_v + g_v D_u)K^2 + D_u D_v K^4\\ &\quad + (f_u b_2 - f_v b_1 - D_u b_2 K^2)\sin(\omega_p t)]\delta U.\end{aligned} \tag{2.10}$$

Finally, the system reduces to the form of a damped, parametrically driven oscillator as follows:

$$\ddot{\delta U} + [\kappa - b_2\sin(\omega_p t)]\dot{\delta U} + \left[\omega_0^2 + 2\alpha\sin(\omega_p t)\right]\delta U = 0, \tag{2.11}$$

where,

$$\kappa = -\left[f_u + g_v - (D_u + D_v)K^2\right] \tag{2.12}$$

$$\omega_0^2 = (f_u g_v - f_v g_u) - (f_u D_v + g_v D_u)K^2 + D_u D_v K^4 \tag{2.13}$$

$$\alpha = \tfrac{1}{2}(f_u b_2 - f_v b_1 - D_u b_2 K^2). \tag{2.14}$$

Equation (2.11) describes an oscillator in which frequency ω_0 and damping κ are modulated by an external forcing term with time dependence $\sin(\omega_p t)$. In absence of forcing terms (i.e., $h = 0$) Eq. (2.11) reduces to a damped harmonic oscillator. On the other hand, when the damping contribution is altogether absent, Eq. (2.11) turns out be the well-known Mathieu equation, extensively used in many areas of physics. It is also apparent that absence of forcing contribution in the damping term leads to an oscillator where the energy storage parameter is modulated at ω_p. The parametrically driven oscillator described by Eq. (2.11) is capable of sustained periodic oscillation. To show this we assume a solution

$$\delta U(t) = A\cos(\omega t + \phi), \tag{2.15}$$

where, A and ϕ are the amplitude and phase of the solution signal wave. Using expansion of $\sin(\omega_p t)$ in Eq. (2.11) and Eq. (2.15) and discarding nonsynchronous terms oscillating at $\omega_p + \omega$ we are led to the following equation;

$$\left(\omega_0^2 - \omega^2 + i\kappa\omega\right)\exp\{i(\omega t + \phi)\} + \left(\frac{b_2\omega}{2} - i\alpha\right) \times \exp\{i(\omega_p t - \omega t - \phi)\} = 0. \tag{2.16}$$

From Eq. (2.16) it follows that sustained oscillation is possible if

$$\omega_p - \omega = \omega \quad or \quad \omega_p = 2\omega \tag{2.17}$$

and

$$\omega^2 - \frac{b_2\omega}{2} - \omega_0^2 = 0; \quad \phi = 0, m\pi \ \ (m = \text{integer}) \tag{2.18}$$

$$\alpha = \kappa\omega. \tag{2.19}$$

From the condition (2.17) the pump frequency ω_p is twice the oscillation frequency ω with oscillation phase $\phi = 0$ or $m\pi$. Let τ be the time period of the output signal, then it can be expressed as $\tau = 4\pi/\omega_p$. The strength of pumping α

must satisfy Eq. (2.19). The last condition is the threshold for oscillation as it ensures a pumping strength necessary to overcome the mean losses (κ) at the threshold. The oscillation frequency ω is generically different from the Hopf frequency, which is given by $\omega_H = \sqrt{4(f_u g_v - g_u f_v) - (f_u + g_v)^2}/2$. It therefore follows from (2.13) and (2.14) that for a given forcing amplitude (h), Eq. (2.19) shows a variation of K^2 with ω_p as follows:

$$K^2 = \frac{b\omega_p(f_u + g_v) + h(f_u g_v - f_v g_u)}{D_u g_v h - b\omega_p(D_u + D_v)}. \tag{2.20}$$

The result (2.20) gives an estimate of the threshold frequency ω_p as a function of K^2 for spatiotemporal instability initiating pattern formation from a homogeneous steady state. We shall use this relation in Sec. IV.

Before concluding this section we mention two pertinent points. First, the present study is for a two-variable system. The question is: Can the treatment be extended to higher number of variables? As the scheme is based on linearization around a steady state, the parametric oscillation can occur in systems with more than two variables, provided the pumping strength exceeds a critical threshold. Casting n-variable linear system of equations in a vector form would be a convenient approach. Second, we have considered forcing of a parameter associated with variable v. This choice is guided by the experimental models like CIMA or Briggs-Rauscher reaction-diffusion system. The parametric oscillation can also be effected by forcing the parameter appearing multiplicatively in the other variable u. However, forcing both u and v may lead to much more complicated mixed-mode oscillations instead of parametric oscillation at multiple frequencies.

III. STABILITY ANALYSIS OF SPATIOTEMPORAL OSCILLATION

We now return to Eq. (2.11) and resort to its perturbative analysis. Our object here is to locate the regions where the system looses its stability with the emergence of pattern forming solutions with growing normal modes. The dynamical equation (2.11) for $\delta U(t)$ can be rewritten in a modified time scale $\tau = \omega_p t$ as follows:

$$\delta\ddot{U} + \epsilon\rho[1 - c\sin(\tau)]\delta\dot{U} + \gamma[1 + \epsilon\sin(\tau)]\delta U = 0, \tag{3.1}$$

where,

$$\epsilon = \frac{2\alpha}{\omega_0^2}, \quad c = \frac{b_2}{\kappa}, \quad \rho = \frac{\kappa\omega_0^2}{2\alpha\omega_p}, \quad \gamma = \frac{\omega_0^2}{\omega_p^2}. \tag{3.2}$$

Equation (3.1) constitutes two time scales for small values of ϵ; the time scale $\xi = \tau$ of the periodic motion itself, and a slower time scale $\eta = \epsilon\tau$, which represents the approach to the periodic motion. Expanding $\delta U(\xi,\eta)$ in a power series in ϵ as

$$\delta U(\xi,\eta) = \delta U_0(\xi) + \epsilon\delta U_1(\xi) + \epsilon^2\delta U_2(\xi) + \ldots \tag{3.3}$$

in Eq. (3.1), the resulting equation can be solved order by order. The zero-order equation of ϵ can be represented as

$$\frac{\partial^2}{\partial\xi^2}(\delta U_0) + \gamma(\delta U_0) = 0, \tag{3.4}$$

which gives a solution of a simple harmonic oscillator with frequency $\sqrt{\gamma}$

$$\delta U_0 = A(\eta)\cos(\sqrt{\gamma}\xi) + B(\eta)\sin(\sqrt{\gamma}\xi). \tag{3.5}$$

For the first order in ϵ and for the special choice $\gamma = \frac{1}{4}$, we have

$$\begin{aligned}\frac{\partial^2}{\partial\xi^2}(\delta U_1) + \gamma(\delta U_1) &= \left[\frac{dA}{d\eta} + \frac{\rho A}{2} + \frac{\rho cB}{4} - \frac{A}{8}\right]\sin\frac{\xi}{2} \\ &- \left[\frac{dB}{d\eta} + \frac{\rho B}{2} + \frac{\rho cA}{4} + \frac{B}{8}\right]\cos\frac{\xi}{2} \\ &+ \left[\frac{\rho cB}{4} - \frac{A}{8}\right]\sin\frac{3\xi}{2} - \left[\frac{\rho cA}{4} - \frac{B}{8}\right]\cos\frac{3\xi}{2}.\end{aligned} \tag{3.6}$$

To avoid secular terms we set the coefficients of $\sin\frac{\xi}{2}$ and $\cos\frac{\xi}{2}$ equal to zero so that we have

$$\begin{pmatrix}\frac{dA}{d\eta}\\ \frac{dB}{d\eta}\end{pmatrix} = \begin{pmatrix}-\frac{\rho}{2} + \frac{1}{8} & -\frac{\rho c}{4}\\ -\frac{\rho c}{4} & -\frac{\rho}{2} - \frac{1}{8}\end{pmatrix}\begin{pmatrix}A\\ B\end{pmatrix}. \tag{3.7}$$

It is clear that A and B have exponential growth. This instability arises because of $\gamma = \frac{1}{4}$ and corresponds to a 2:1 subharmonic resonance in which the driving frequency (ω_p) is twice the natural frequency (ω_0). Expanding γ in a power series in ϵ one obtains

$$\gamma = \tfrac{1}{4} + \epsilon\gamma_1 + \epsilon^2\gamma_2 + \cdots. \tag{3.8}$$

Repeating the same calculation with this γ, we get some additional terms in Eq. (3.7), which can be solved by assuming a solution in the form $A(\eta) = A_0 exp(\eta\Lambda)$, $B(\eta) = B_0 exp(\eta\Lambda)$. For nontrivial constants A_0 and B_0, the following condition must hold

$$\begin{vmatrix}-\frac{\rho}{2} + \frac{1}{8} - \Lambda & -\frac{\rho c}{4} + \gamma_1\\ -\frac{\rho c}{4} - \gamma_1 & -\frac{\rho}{2} - \frac{1}{8} - \Lambda\end{vmatrix} = 0. \tag{3.9}$$

The eigenvalues $\Lambda_\pm$ are given by $\Lambda_\pm = -\frac{\rho}{2} \pm \sqrt{\frac{\rho^2c^2}{16} - \gamma_1^2 + \frac{1}{64}}$. For the transition between stable and unstable regions, we set $\Lambda_\pm = 0$, and obtain $\gamma_1 = \sqrt{\frac{\rho^2c^2}{16} - \frac{\rho^2}{4} + \frac{1}{64}}$. The condition gives the two transition curves emerging from $\gamma = \frac{1}{4}$ forming instability region in the form of a V-shaped Arnold's-tongue-like profile in the ϵ-γ plane, outside which the system shows quasiperiodic motion. γ is therefore modified up to first order as follows:

$$\gamma = \frac{1}{4} \pm \epsilon\sqrt{\frac{\rho^2c^2}{16} - \frac{\rho^2}{4} + \frac{1}{64}}. \tag{3.10}$$

Keeping in mind that $\alpha, \omega_0^2, \kappa$ are all dependent on wavelength one can plot γ vs. K^2 for selected parameter values and find that for a given ω_p, there is a particular permissible range of K^2 for a specific γ. The pattern formation out of a homogeneous steady state due to instability may therefore occur for this allowed range of wave numbers. Second, the stable and unstable regions and the associated boundaries for a given range of K^2 can be captured from the variation

of γ as a function of ϵ according to Eq. (3.10) depicting the V-shaped region. The region within the V-shaped curve, i.e., within the tonguelike structure is due to the exponential growth of the solution, which is responsible for the emergence of temporally oscillating patterns. The outside region corresponds to the stable quasiperiodic domain. A further clarification regarding the V-shaped region is in order. It is well known that the amplitude-frequency characteristics depicting Arnold's tongue refers to the situation when the system's characteristic frequency is a Hopf frequency. The parametric oscillation at frequency ω in the present case is determined by the forcing frequency ω_p through the relation (2.17). While the Hopf frequency depends only on the system parameters, the parametric oscillation frequency ω exists for every ω_p and oscillation takes place provided the threshold condition (2.19) is maintained. However, as the perturbative analysis in the two cases are parallel, we have referred to the V-shaped curve as a tonguelike structure. We illustrate these issues with the help of two examples in detail in the following section.

IV. EXAMPLES AND NUMERICAL SIMULATIONS

A. CIMA reaction-diffusion model

The Lengyel-Epstein model [23–25] for CIMA reaction-diffusion system [30] can be described in dimensionless form as follows;

$$\frac{\partial u}{\partial t} = a - u - \frac{4uv}{1+u^2} + \nabla^2 u \tag{4.1}$$

$$\frac{\partial v}{\partial t} = \sigma\left[\tilde{b}\left(u - \frac{uv}{1+u^2}\right) + d\nabla^2 v\right]. \tag{4.2}$$

Here u and v refer to the concentrations of intermediates I^- and ClO_2^-, respectively. a and $\tilde{b}$ are the parameters, which

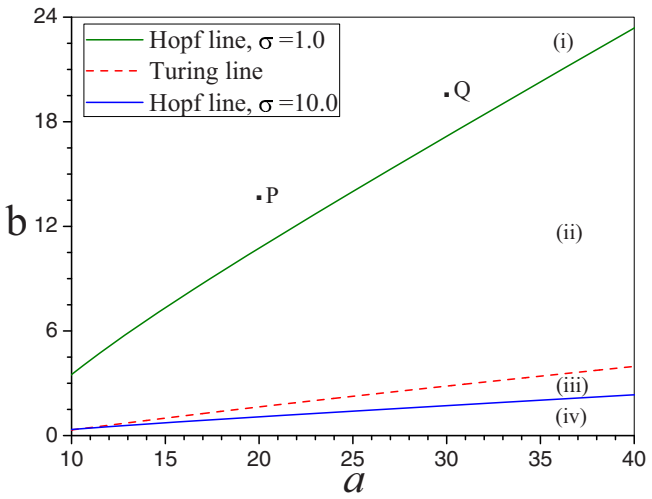

FIG. 1. Parameter space for undriven CIMA model. Region (i) shows steady-state domain. Region (ii) remains oscillatory with respect to green Hopf line (for $\sigma = 1.0$) but steady-state domain with respect to blue Hopf line (for $\sigma = 10.0$). Region (iii) between Turing and blue Hopf line stands for Turing pattern forming domain. Region (iv) represents oscillatory domain with respect to both the Hopf lines.

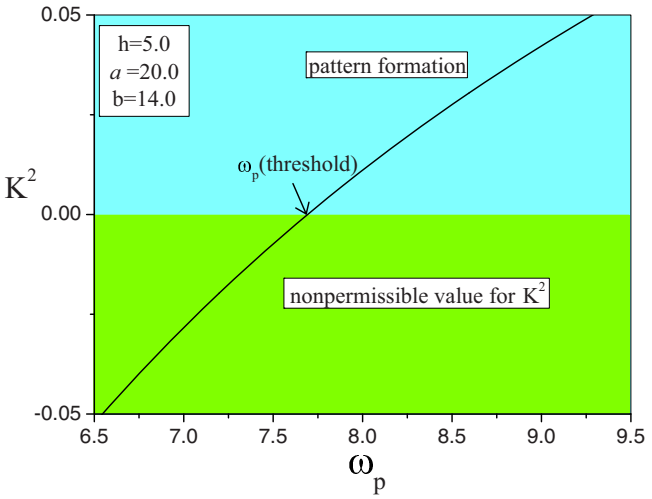

FIG. 2. Estimation of $\omega_p(threshold)$ of parametric oscillation; K^2 vs. ω_p curve plotted for the steady state $P(a,b) = (20,14)$ shown in Fig. 1 according to Eq. (2.20) for $D_v/D_u = 1.5$ and $h = 5.0$ for CIMA reaction-diffusion model.

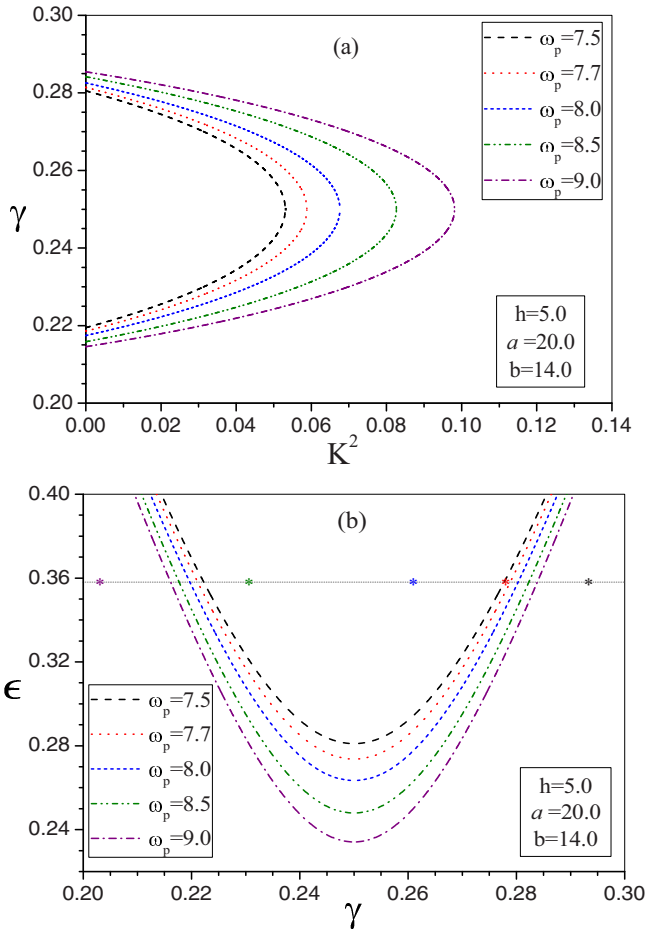

FIG. 3. (a) Estimation of the range of unstable modes using Eq. (3.10); γ vs. K^2 curve. (b) Location of the region of spatiotemporal oscillation within V-shaped or Arnold's-tongue-like region; ϵ vs. γ curve for the parameters (as mentioned in the figure) for CIMA reaction-diffusion system.

depend on rate constants and the concentrations of the slow reactants. d is the ratio of two diffusion coefficients, D_v/D_u. σ is a parameter that characterizes the strength of complexation of an iodide ion with an external complexing agent such as starch or polyvinyl alcohol. To explore parametric oscillation we make $\tilde{b}$ a time-dependent function $\tilde{b}(t) = b + h\sin(\omega_p t)$, where h and ω_p are the strength and frequency of the modulating field, respectively.

The linear stability analysis of the system (4.1) and (4.2) with constant b is well known [31,32]. By varying the concentration of the complexing agent, i.e., by adjusting σ one can control (Fig. 1) the Hopf bifurcation line in such a way in a-b parameter space that it lies above or below the Turing line (shown as dotted line), which is independent of σ. In Fig. 1 we have separated out the various regions in the parameter space. The region (i) separated from the oscillatory region (ii) by Hopf bifurcation boundary line for $\sigma = 1.0$ comprises the stable steady-state domain of the system. With increase of σ from 1.0 to 10.0, the Hopf line shifts downwards (the blue one). As it crosses the Turing line and lies below it, one encounters the region (iii) in between the Turing and Hopf line, which corresponds to the region of diffusion-induced instability or the region of stationary Turing pattern. Below the Hopf line at $\sigma = 10.0$, we have the usual limit cycle region (iv). Two representative points, namely, P and Q in the homogeneous steady-state region (i) are shown in Fig. 1. Our object is to look for spatiotemporal instability due to a periodic perturbation of parameter b on these steady states.

To proceed further we now choose the steady state P in the region (i) for which $a = 20.0$, $b = 14.0$. The other parameters corresponding to Fig. 1 are $\sigma = 1.0$, $d = 1.5$. We then switch on the temporal perturbation $h\sin(\omega_p t)$ on the parameter b by setting $h = 5.0$. A closer look at our earlier analysis in Sec. II clearly suggests that the driving frequency ω_p must exceed a $\omega_p(threshold)$ for which K^2 is positive and the condition $\omega_p = 2\omega$ [Eq. (2.17)] is maintained. For the parameter set as mentioned $\omega_p(threshold)$ can be obtained from a plot of K^2 vs. ω_p using Eq. (2.20), which, in turn, is the threshold condition (2.19) for parametric oscillation. It is apparent from the change of sign of K^2 that the threshold frequency $\omega_p = 7.7$. Therefore, only for $\omega_p \geqslant \omega_p(threshold)$ the strength of the field is strong enough to induce spatiotemporal parametric oscillation at $\omega = \omega_p/2$.

Figure 2 does not give any upper bound for ω_p and also the allowed range of K^2. However, these can be obtained from the perturbative analysis of spatiotemporal instability as carried out in Sec. III. To this end we take resort to perturbative estimate of γ [Eq. (3.10)] and plot in Fig. 3(a) γ as a function of K^2 for the aforesaid parameters for several values of ω_p. It is apparent that with increase of ω_p the range of K^2 increases for a specific value of γ. In order to locate the region of spatiotemporal oscillation we now plot ϵ vs. γ according to (3.10) for several values of ω_p and for $K^2 = 0.01$. The results

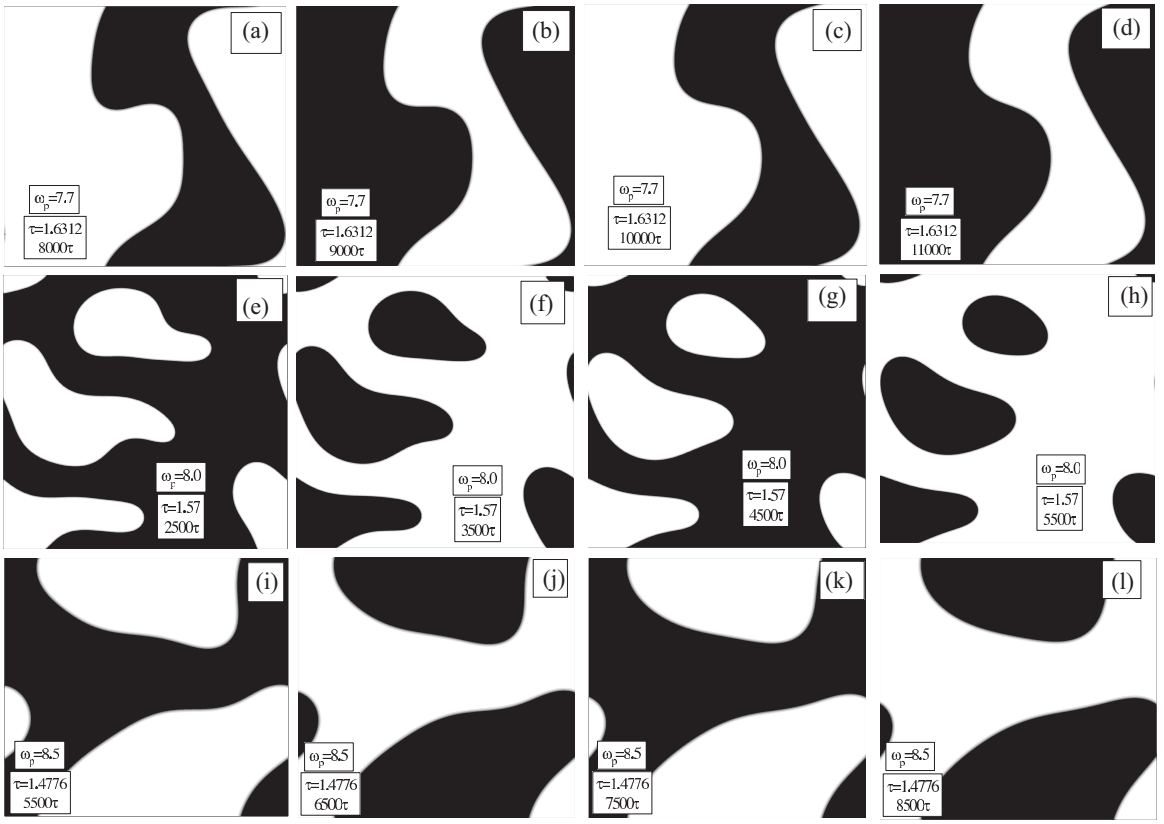

FIG. 4. Standing clusters: Parametric spatiotemporal oscillatory patterns of u induced by sinusoidal perturbation $h\sin(\omega_p t)$ [above $\omega_p(threshold)$] with $h = 5.0$ on the steady state P ($a = 20.0$, $b = 14.0$) shown in Fig. 1 for three sets of ω_p values for the parametric set as mentioned in the text for CIMA reaction-diffusion model. White corresponds to high concentration of u. For each set (for a fixed ω_p) snapshots are taken at definite interval of time period $\tau(= 4\pi/\omega_p)$, of the parametric oscillation.

are displayed [Fig. 3(b)] as typical V-shaped regions in the form of well-known Arnold's tongues, which separate out the oscillatory region from the rest of the parameter space. For convenience, we now locate five points (asterisk marked) on a line at $\epsilon = 0.357$ in the ϵ-γ parameter space corresponding to five values of ω_p [note that $\epsilon = 2\alpha/\omega_0^2$, where ω_0^2 and α are defined in Eqs. (2.14) and (2.14), respectively and $\gamma = \omega_0^2/\omega_p^2$ according to (3.2)]. When ω_p is 7.5 i.e., below $\omega_p(threshold)$ the point lies outside the corresponding V-shaped region. At $\omega_p = \omega_p(threshold)$ $(= 7.7)$, it crosses the boundary to enter into the spatiotemporal unstable region responsible for exponential growth. When $\omega_p = 9.0$ the phase point crosses of the boundary of the corresponding V-shaped profile to escape out the oscillatory region. Thus with increase of ω_p, the position of γ moves from right to left in the ϵ-γ plane and only when the points remain inside the tongue profile the dynamical system undergoes spatiotemporal oscillation induced by parametric modulation of the scaling parameter.

In order to corroborate the above theoretical analysis we now carry out full numerical simulations of Eqs. (4.1) and (4.2) with explicit Euler method following discretization of space and time. A finite system size of 1000×1000 points with periodic boundary conditions has been chosen. A time interval $\Delta t = 0.0025$ and a cell size $\Delta x = \Delta y = 2.5$ have been found to be appropriate for this purpose. The parametric modulation of b is performed on the stable steady state P of Fig. 1 ($a = 20.0$, $b = 14.0$) with a fixed value of $h = 5.0$ for the parameter set $\sigma = 1.0$, $d = 1.5$. The numerical simulation results have been obtained for five sets of ω_p values corresponding to Fig. 3. At $\omega_p = 7.5$, i.e, below $\omega_p(threshold)$ the system remains homogeneous. In Fig. 4 we have presented three horizontal panels for u corresponding to $\omega_p = 7.7$, 8.0, and 8.5. The snapshot of each profile of u of a particular panel is obtained at an interval of 1000τ time unit ($\tau = 4\pi/\omega_p$). Each horizontal panel suggests that at every interval of 2000τ time units, the pattern repeats. During 1000τ time period the regions that were dark in the earlier period becomes bright. This finding is reminiscent of the standing clusters [22] characterized

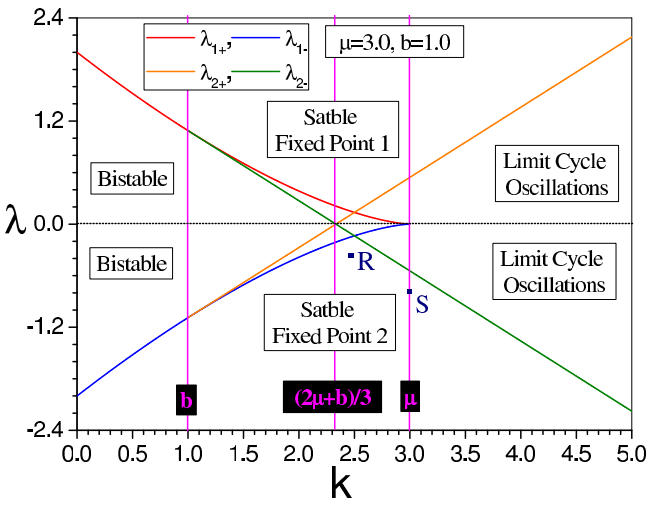

FIG. 5. Cross-shaped diagram for parameter space of undriven Briggs-Rauscher reaction for $\mu > b$, showing stable fixed point region, the bistable regions and the limit cycle oscillatory regions.

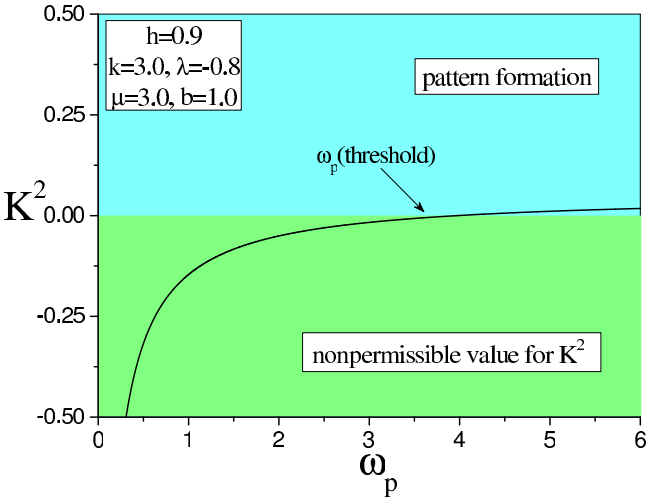

FIG. 6. Estimation of $\omega_p(threshold)$ of parametric oscillation; K^2 vs. ω_p curve plotted for the stable steady state $S(k = 3.0, \lambda = -0.8)$ of Fig. 5 according to Eq. (2.20) with $\mu = 3.0$, $b = 1.0$, $D_u = 1.0$, $D_v = 10.0$, and $h = 0.9$ for Briggs-Rauscher reaction-diffusion model.

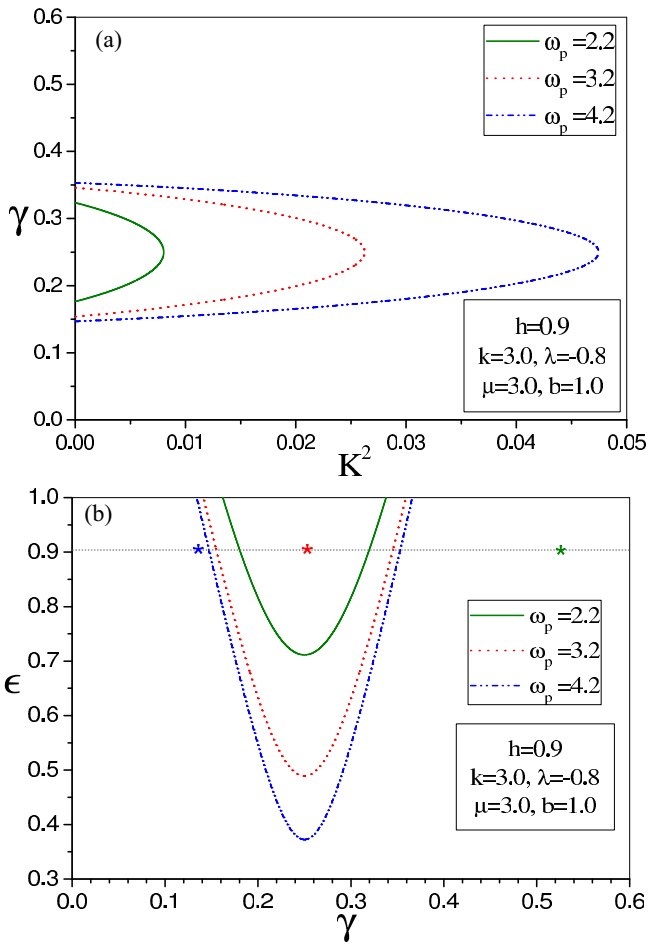

FIG. 7. (a) Estimation of the range of unstable modes using Eq. (3.10); γ vs. K^2 curve. (b) Location of the region of spatiotemporal oscillation within V-shaped tonguelike region; ϵ vs. γ curve for the parameters (as mentioned in the figure) for Briggs-Rauscher reaction-diffusion model.

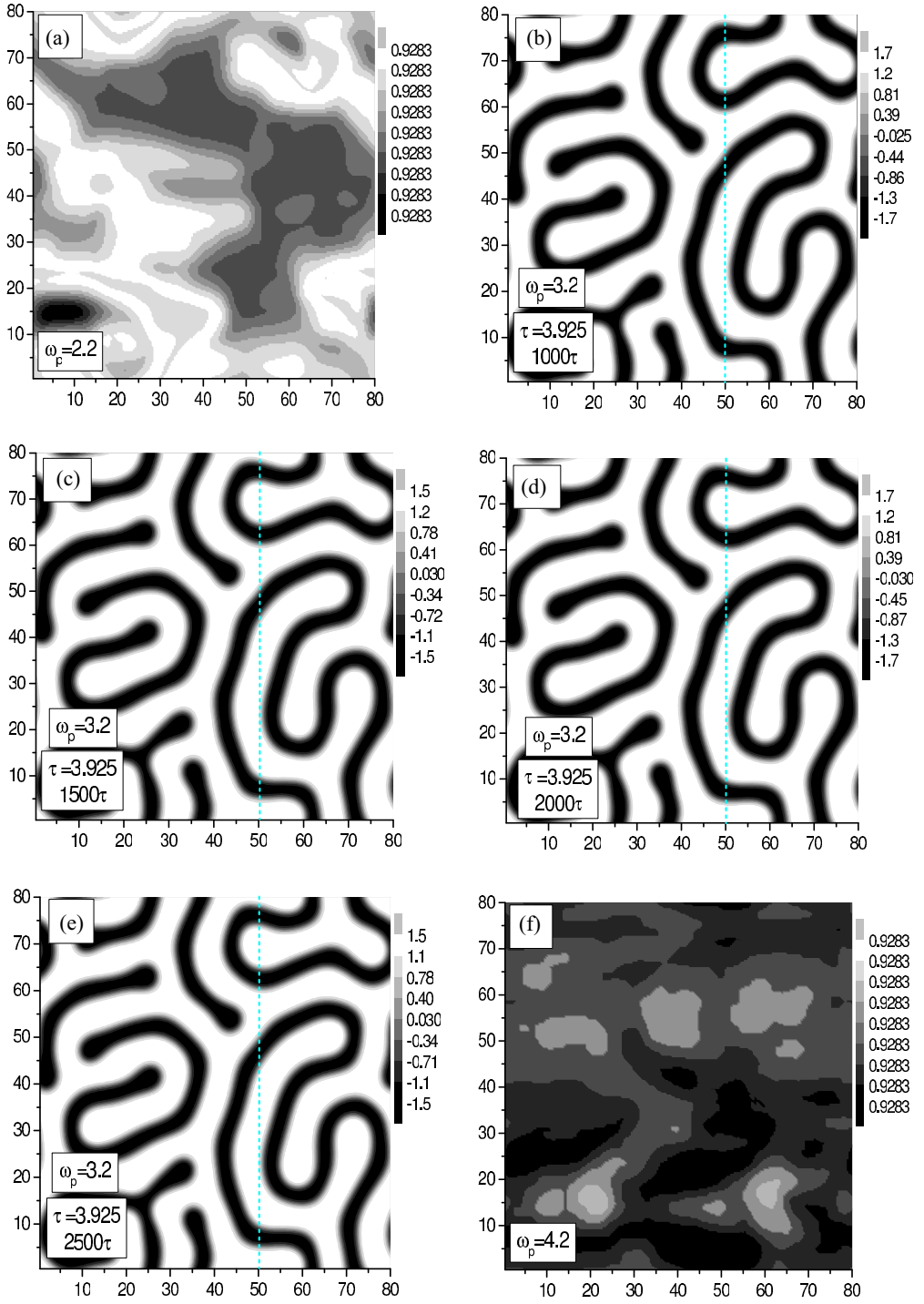

FIG. 8. Breathing patterns: Parametric spatiotemporal profiles of u induced by sinusoidal perturbation $h\sin(\omega_p t)$ with $h = 0.9$ on the steady state $S(k = 3.0, \lambda = -0.9)$ of Fig. 5 for $\mu = 3.0$, $b = 1.0$ for Briggs-Rauscher reaction model. (a) $\omega_p = 2.2$ [below $\omega_p(threshold)$] showing homogeneous state, (b)–(e) $\omega_p = 3.2$ [above $\omega_p(threshold)$] showing snapshots at an interval of 500τ (with $\tau = 4\pi/\omega_p$). Turing-like labyrinth breathes periodically in time (f) $\omega_p = 4.2$ (outside V-shaped or tonguelike region); the system returns to homogeneous state.

by fixed spatial domains that oscillate periodically in time (and occupy the entire medium), a scenario, experimentally observed earlier in the BZ reaction by incorporating the effect of global feedback. At $\omega_p = 9.0$ the system comes out of the V-shaped region and returns to homogeneous state confirming our theoretical prediction.

B. Briggs-Rauscher reaction-diffusion model

A simple analytical model for designing a chemical oscillator that captures the behavior of oscillating iodine clock reaction or Briggs-Rauscher reaction [27] was suggested by Boissonade and De Kepper [28]. The governing reaction-

diffusion equations for the two species u and v are

$$\dot{u} = -u^3 + \mu u - kv - \lambda + D_u \nabla^2 u \tag{4.3}$$

$$\dot{v} = \tilde{b}(u - v) + D_v \nabla^2 v, \tag{4.4}$$

where μ, k are the positive parameters [33]. However, parameter λ can assume positive or negative value. $\tilde{b}$ is the reciprocal of characteristic evolution time $\tilde{\tau}$ of the feedback, where $\tilde{b} = b + h\sin(\omega_p t)$. Linear stability analysis for $h = 0.0$ is well known for homogeneous system [28] and shows that depending on whether $\mu > b$ or $\mu < b$, phase space of the dynamical system can be divided into separate regions. For $\mu > b$ the phase space is composed of bistable, stable steady state and limit cycle oscillation regions as depicted in Fig. 5. It is apparent from Fig. 5 that for $k < b$ and $\lambda_{1-} < \lambda < \lambda_{1+}$ there are two stable solutions (bistable regions) where $\lambda_{1\pm} = \pm 2[(\mu - k)/3]^{3/2}$. For $b < k < (2\mu + b)/3$ the system is bistable for $\lambda_{2-} < \lambda < \lambda_{2+}$ where $\lambda_{2\pm} = \pm\frac{1}{3}[(\mu - b)/3]^{1/2}[3k - 2\mu - b]$. For $\lambda > |\lambda_{2\pm}|$ there is only one stable solution (stable fixed point regions). For $k > (2\mu + b)/3$ and $\lambda_{2-} < \lambda < \lambda_{2+}$ the system has only unstable steady state, which undergoes limit cycle oscillations. For $(2\mu + b)/3 < k < \mu$ and $\lambda < |\lambda_{1\pm}|$ the system has three unstable steady states solutions; for other values of λ there is only stable fixed point regions. Two representative fixed points R and S as marked in the region of negative λ of Fig. 5 are shown as stable steady states.

Having depicted in Fig. 5 the various stability zones in the λ-k parameter space for the undriven system ($h = 0.0$), we first select the steady state $S(k,\lambda) = (3.0, -0.8)$ and switch on the perturbation $h\sin(\omega_p t)$ on the scaling parameter to explore parametric spatiotemporal oscillation initiating pattern formation. To this end we first set $\mu = 3.0, b = 1.0, D_u = 1.0$, and $D_v = 10.0$ for the rest of the calculations. The strength of modulation is fixed at $h = 0.9$ and we look for $\omega_p(threshold)$ as in the previous example. Making use of the condition (2.20) a plot of K^2 vs. ω_p as shown in Fig. 6 suggests the value of $\omega_p(threshold)$.

Next we look for the allowed ranges of K^2 and the region of unstable growth of the system modes lying within the V-shaped region with help of Eqs. (3.2) and (3.10). In Fig. 7(a) the variation of γ as a function of K^2 for several values of ω_p around $\omega_p(threshold)$ is displayed. We observe as before that the range of K^2 for a given γ becomes wider for higher values of ω_p. The passage of the dynamical system into the unstable region (V-shaped profile) with change of ω_p from below to above threshold values is shown in Fig. 7(b) in terms of the plot of ϵ vs. γ for $K^2 = 0.001$. The three star marked points lying on a straight line for $\epsilon = 0.901$ in the figure corresponding to these ω_p values clearly reveal that when $\omega_p = 2.2$, the point lies outside the tongue. With increase of ω_p the point shifts from right to left and only when the point lies within the V-shaped region the system exhibits instability. At $\omega_p = 4.2$ the system comes out of the boundary and escapes the region.

In order to corroborate the aforesaid analysis we now carry out numerical simulations of Eqs. (4.3)–(4.4) with explicit Euler method for a finite system size of 80×80 points with periodic boundary conditions. The time interval $\Delta t = 0.0025$ and a cell size $\Delta x = \Delta y = 0.4$ have been found to be appropriate for this purpose. The results are plotted in Fig. 8

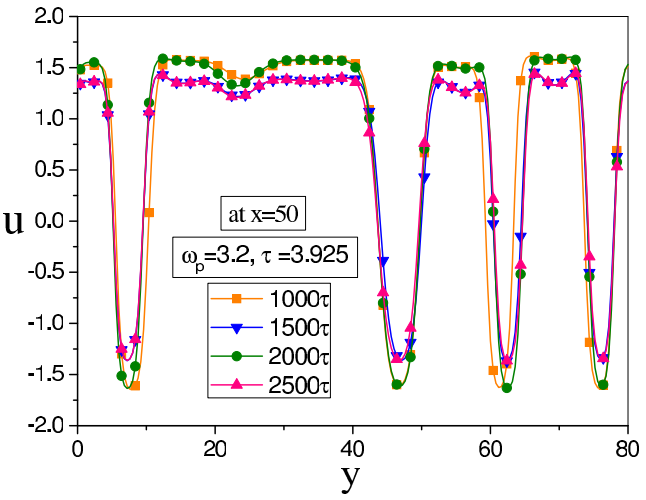

FIG. 9. Snapshots at an interval of 500τ for the spatial variation of concentration variable u vs. y at a fixed $x = 50$ of Briggs-Rauscher reaction-diffusion model [u values lie along the blue dotted line as indicated in Figs. 8(b)–8(e)] showing periodic breathing.

for three values of ω_p. Figure 8(a) shows the homogeneous profile of u for $\omega_p = 2.2$ [below $\omega_p(threshold)$] stationary in time. Figures 8(b)–8(e) represent the snapshots of Turing type labyrinths of u for $\omega_p = 3.2$. These stripes breath slowly at regular interval of 500τ. To make this time-periodic breathing more prominent we have taken snapshots at a regular time interval of 500τ for the variation of the concentration variable u as a function of y for a fixed x [the selected u values lie on the dotted blue line in Figs. 8(b)–8(e)] in Fig. 9. Each profile of u repeats at an interval of 1000τ. This breathing clearly demonstrates parametric spatiotemporal oscillatory patterns. Again, at $\omega_p = 4.2$, i.e., when the system is outside the V-shaped region the system becomes homogeneous altogether [Fig. 8(f)], vindicating our theoretical analysis. We point out in passing that the nature of the pattern remains unaffected by the change of boundary condition (from periodic to zero flux). Patterns are, however, sensitive to the variation of initial condition, i.e., the location of the steady state. This is not unexpected in view of the fact that although our linear analysis and the multiscale perturbation theory predict the spatiotemporal parametric threshold, the nature of the pattern type, which depends on the specificity of nonlinearity of the kinetics and the extent of departure from the threshold, remains outside the scope of our scheme.

V. CONCLUSION

We have considered a reaction-diffusion system in a homogeneous steady state. When subjected to a time-periodic perturbation of a scaling parameter, the dynamical system undergoes spatiotemporal oscillation, beyond a critical threshold frequency of the perturbation, which fixes the range of allowed modes for the spatially stationary but temporally oscillating patterns. A multiscale perturbation analysis of this scenario clearly reveals the domain of instability within a V-shaped region similar to Arnold's tongue in an amplitude-frequency plot. The main conclusions of this study can be summarized as follows.

(i) Forcing a dynamical system that remains in a Hopf state can be well described by an amplitude equation in the form of Ginzburg-Landau equation. This is, however, not appropriate for understanding the present situation as the dynamical state in absence of perturbation remains in a steady state. A linearized description such as Eq. (2.11) is sufficient and can be used for other examples. Second, it should be noted that an amplitude equation based approach for analysis of the emergence of spatiotemporal instability and patterns is not advantageous because the parametric oscillation is generically distinct from usual Hopf oscillation. The difference lies in the fact that in the latter case the dynamical system has an unique threshold (Hopf bifurcation threshold) while the threshold for parametric oscillation depends on the frequency and amplitude of forcing and this makes the choice of perturbation parameter (ϵ in our case) difficult since for every threshold there exists a perturbation parameter. For this reason we have chosen this parameter as a ratio, $2\alpha\omega/\omega_0^2$, which is a frequency ratio associated with oscillation threshold and characteristic oscillation frequency. For ideal validity of the perturbation expansion it is necessary to keep $\epsilon \ll 1$ throughout the treatment.

(ii) The parametrically driven damped linear oscillator [Eq. (2.11)] can effectively capture the underlying physics of instability that results in temporally breathing and spatially localized patterns in the form of standing clusters and temporal breathers observed in full numerical simulation of the models. The parameters of the oscillator, e.g., frequency, damping, amplitude of forcing depend on the wavelength of excitation ($K \neq 0$). It is also apparent that in the studies of the two models the pattern types are different although they originate from a generic parametric spatiotemporal instability. In the case of standing clusters the patterns look irregular while the breathers are typical stripes with characteristic wavelengths. We believe that this is due to nature of nonlinearity of the models concerned. It is therefore not difficult to anticipate that other models may lead to different pattern types when they are subjected to parametric instability. These patterns are generically distinct from what one observes for Turing patterns or other patterns observed under forced condition.

(iii) The dependence of the range of allowed values of wavelength (K^2) on the excitation frequency (ω_p) beyond the critical threshold for oscillation as well as the scaled amplitude-frequency plot depicting a V-shaped tongue reveal the key aspects of parametric instability of spatially localized patterns.

(iv) A simple variant of the general scheme presented in Sec. II can be considered by bringing in the parametric modulation in the G_u term of Eq. (2.4), instead of the scaling factor $\tilde{b}$. The pattern types can be explored by numerical simulation of the relevant model.

Time-periodic forcing by light in a number of chemical reactions has been investigated successfully in the recent past on several occasions. We believe that parametric oscillation of the stationary pattern can be observed by proper choice of the parameters required for fixing the appropriate conditions for instability in these models.

ACKNOWLEDGMENTS

Thanks are due to the Council of Scientific and Industrial Research, Government of India, for partial financial support [Ref. No. 09/080(0885)/2013-EMR-I].

[1] V. Petrov, Q. Ouyang, and H. L. Swinney, Nature (London) **388**, 655 (1997); M. Dolnik, A. M. Zhabotinsky, and I. R. Epstein, Phys. Rev. E **63**, 026101 (2001).

[2] M. Dolnik, I. Berenstein, A. M. Zhabotinsky, and I. R. Epstein, Phys. Rev. Lett. **87**, 238301 (2001); K. Martinez, A. L. Lin, R. Kharrazian, X. Sailer, and H. L. Swinney, Physica D **168-169**, 1 (2002); S. Ghosh and D. S. Ray, J. Chem. Phys. **143**, 124901 (2015).

[3] C. A. Czeisler, J. S. Allan, S. H. Strogatz, J. M. Ronda, R. Sanchez, C. D. Rìos, W. O. Freitag, G. S. Richardson, and R. E. Kronauer, Science **233**, 667 (1986).

[4] L. Glass, Nature (London) **410**, 277 (2001); C. Gronfier, K. P. Wright, Jr., R. E. Kronauer, and C. A. Czeisler, Proc. Natl. Acad. Sci. USA **104**, 9081 (2007).

[5] K. P. Wright, Jr., A. W. McHill, B. R. Birks, B. R. Griffin, T. Rusterholz, and E. D. Chinoy, Curr. Biol. **23**, 1554 (2013); T. Roenneberg, C. J. Kumar, and M. Merrow, *ibid.* **17**, R44 (2007).

[6] A. L. Lin, M. Bertram, K. Martinez, H. L. Swinney, A. Ardelea, and G. F. Carey, Phys. Rev. Lett. **84**, 4240 (2000); V. K. Vanag, A. M. Zhabotinsky, and I. R. Epstein, *ibid.* **86**, 552 (2001).

[7] A. L. Lin, A. Hagberg, E. Meron, and H. L. Swinney, Phys. Rev. E **69**, 066217 (2004).

[8] A. Yochelis, A. Hagberg, E. Meron, A. L. Lin, and H. L. Swinney, SIAM. J. Appl. Dyn. Syst. **1**, 236 (2002).

[9] O. Steinbock, V. Zykov, and S. C. Müller, Nature (London) **366**, 322 (1993); R.-M. Mantel and D. Barkley, Phys. Rev. E **54**, 4791 (1996).

[10] A. Karma and V. S. Zykov, Phys. Rev. Lett. **83**, 2453 (1999); A. L. Lin, A. Hagberg, A. Ardelea, M. Bertram, H. L. Swinney, and E. Meron, Phys. Rev. E **62**, 3790 (2000).

[11] I. Sgura, B. Bozzini, and D. Lacitignola, AIP Conf. Proc. **1493**, 896 (2012).

[12] M. Eiswirth and G. Ertl, Phys. Rev. Lett. **60**, 1526 (1988); S. Rüdiger, D. G. Míguez, A. P. Muñuzuri, F. Sagués, and J. Casademunt, *ibid.* **90**, 128301 (2003); S. Ghosh and D. S. Ray, Eur. Phys. J. B **88**, 180 (2015).

[13] Q. Gao, J. Li, K. Zhang, and I. R. Epstein, Chaos **19**, 033134 (2009); J. Porter, I. Tinao, A. Laverón-Simavilla, and J. Rodríguez, Phys. Rev. E **88**, 042913 (2013); A. O. León, M. G. Clerc, and S. Coulibaly, *ibid.* **91**, 050901 (2015).

[14] V. Petrov, S. K. Scott, and K. Showalter, J. Chem. Phys. **97**, 6191 (1992); D. G. Míguez, S. Alonso, A. P. Muñuzuri, and F. Sagués, Phys. Rev. Lett. **97**, 178301 (2006).

[15] M. I. Español and H. G. Rotstein, Chaos **25**, 064612 (2015).

[16] I. Berenstein and Y. De Decker, J. Chem. Phys. **143**, 064105 (2015).

[17] V. K. Vanag and I. R. Epstein, Phys. Rev. E **73**, 016201 (2006); P. Ghosh, S. Sen, and D. S. Ray, *ibid.* **79**, 016206 (2009); P. Ghosh and D. S. Ray, J. Chem. Phys. **135**, 104112 (2011).

[18] R. Gallego, D. Walgraef, M. San Miguel, and R. Toral, Phys. Rev. E **64**, 056218 (2001); A. Yochelis, C. Elphick, A. Hagberg, and E. Meron, Physica D **199**, 201 (2004).
[19] Y. Kuramoto, *Chemical Oscillations, Waves, and Turbulence* (Springer, Berlin, 1984).
[20] M. Cross and H. Greenside, *Pattern Formation and Dynamics in Nonequilibrium System* (Cambridge University Press, Cambridge, 2009).
[21] D. G. Mìguez, E. M. Nicola, A. P. Muñuzuri, J. Casademunt, F. Saguès, and L. Kramer, Phys. Rev. Lett. **93**, 048303 (2004).
[22] V. K. Vanag, L. Yang, M. Dolnik, A. M. Zhabotinsky, and I. R. Epstein, Nature (London) **406**, 389 (2000).
[23] I. Lengyel, G. Rábai, and I. R. Epstein, J. Am. Chem. Soc. **112**, 9104 (1990).
[24] I. Lengyel and I. R. Epstein, Science **251**, 650 (1991).
[25] I. Lengyel, S. Kádár, and I. R. Epstein, Science **259**, 493 (1993).
[26] S. S. Riaz and D. S. Ray, J. Chem. Phys. **123**, 174506 (2005); S. Sen, P. Ghosh, S. S. Riaz, and D. S. Ray, Phys. Rev. E **81**, 017101 (2010).
[27] T. S. Briggs and W. C. Rauscher, J. Chem. Educ. **50**, 496 (1973).
[28] J. Boissonade and P. de Kepper, J. Phys. Chem. **84**, 501 (1980).
[29] M. Braune and H. Engel, Chem. Phys. Lett. **211**, 534 (1993); H. Wang, K. Zhang, and Q. Ouyang, Phys. Rev. E **74**, 036210 (2006).
[30] V. Castets, E. Dulos, J. Boissonade, and P. De Kepper, Phys. Rev. Lett. **64**, 2953 (1990).
[31] S. H. Strogatz, *Nonlinear Dynamics and Chaos* (Westview Press, Boulder, 1994).
[32] I. R. Epstein and J. A. Pojman, *An Introduction to Nonlinear Chemical Dynamics* (Oxford University Press, Oxford, 1998).
[33] In this abstract model, the concentrations u and v can be negative. It is, however, possible [N. Samardzija, L. D. Greller, and E. Wasserman, J. Chem. Phys. **90**, 2296 (1989)] to transform Eqs. (4.3)–(4.4), to another pair of variables that remain nonnegative. The exercise, however, is not needed for our present purpose.